



# 3D Spatial Interpolation Methods for Open-Pit Mining Air Quality with Data Acquired by Small UAV Based Monitoring System

Nguyen QUOC LONG<sup>1,\*</sup>, Cao XUAN CUONG<sup>1</sup>, Le VAN CANH<sup>1</sup>,  
Nguyen NGOC BICH<sup>2</sup>, Dang AN TRAN<sup>3</sup>, Le QUI THAO<sup>4</sup>, Xuan-Nam BUI<sup>4</sup>

<sup>1</sup>) Department of Mine Surveying, Hanoi University of Mining and Geology, Hanoi, Vietnam; email: nguyenquoclong@humg.edu.vn; caoxuancuong@humg.edu.vn; levancanh@humg.edu.vn

<sup>2</sup>) Department of Occupational Health and Safety, Hanoi University of Public Health, Hanoi, Vietnam; email: nnb@huph.edu.vn

<sup>3</sup>) Department of Water Resources Engineering, Thuyloi University, Hanoi, Vietnam; email: antd@tlu.edu.vn

<sup>4</sup>) Department of Surface Mining, Hanoi University of Mining and Geology, Hanoi, Vietnam; email: buixuannam@humg.edu.vn

<http://doi.org/10.29227/IM-2020-02-32>

Submission date: 06-03-2020 | Review date: 22-09-2020

## Abstract

Open-pit mining activities, including blasting, drilling, loading, and transport, often result in the direct emission of particulates and gases into the atmosphere. Occupational exposure to these pollutants is considered as the risk for health, especially the risk of developing respiratory diseases. An air quality monitoring system and spatial analysis are necessary to identify these potential hazards. In this study, we propose an air quality monitoring system that integrates gas and dust sensors into a small multi-rotor copter or unmanned aerial vehicle (UAV). Different spatial interpolation methods including trilinear interpolation, nearest neighbour, and natural neighbour applied to the monitoring data (CO, SO<sub>2</sub>, PM2.5, CO<sub>2</sub>) from our system to derive air concentration levels in the atmosphere of open-pit coal mines were also examined. The results show that the UAV based air quality monitoring system performed efficiently and safely in conditions of deep open-pit coal mines. In addition, for the estimation of the concentration level of gases and dust in unsampled points, trilinear interpolation performed with the most accurate result, followed by natural neighbor and nearest neighbor.

**Keywords:** air quality, open-pit mines, spatial interpolation, UAV-MSC

## 1. Introduction

Mining industry plays a crucial role in the socio-economic development, especially for many developing countries across the world. However, it often causes severe environmental issues (Chen et al., 2019; J. Long et al., 2018). Mining activities often produce different air pollutant sources such as particulate matters (PM<sub>10</sub>, PM<sub>2.5</sub> and PM<sub>1.0</sub>) (Arregocés et al., 2018), hazardous substances (sulfur dioxide (SO<sub>2</sub>), carbon dioxide (CO<sub>2</sub>), carbon monoxide (CO)), and heavy metals (Espitia-Pérez et al., 2018; J. Long et al., 2018). Air pollutant in mining sites not only affects directly to occupational health within mining areas (Grozdanovic et al., 2018; León-Mejía et al., 2011; Petsonk et al., 2013) but also increases environmental and health problems in the surrounding regions (Hendryx et al., 2020; Pandey et al., 2014; Zhang et al., 2020).

To prevent air pollution and reduce health-related issues, it is essential to accurately observe and predict the spatio-temporal distribution of air quality in mining areas, particularly in the small space with heavy air pollution like open-pit coal mines (Alvarado et al., 2015). As various hazardous compositions emitting to the atmosphere, different methods have been used to observe air quality, including manual analysis, concentration meter, and continuous analyzer (Chang et al., 2020; Dieu Hien et al., 2019; Yang et al., 2020). However, these methods are generally time-consuming and costly practices, so they are often unaffordable for many developing countries. With the advanced development of unmanned aerial vehicle (UAV) technology in recent years, UAV has been applied in different mining activities including pit and dump manage-

ment (Padró et al., 2019), stockpile computation (Le, 2020; Ravea et al., 2016), blast-induced ground vibration (X.-N. Bui et al., 2020), and 3D mapping open-pit mines (D. T. Bui et al., 2017; N. Q. Long et al., 2019; Nghia, 2020). In the field of mining environment management, it is noted that UAV carrying modular gas sensors is an effective monitoring system of air quality (Rohi et al., 2020). A UAV monitoring system can help to observe the vertical distribution of air quality accurately (Liu et al., 2020; Sheng et al., 2019) with acceptable prices, especially within the open-pit mining areas where a complex ground surface and unstable geomorphology is common (Alvarado et al., 2015; Liu et al., 2020; Villa et al., 2016). However, there are often limitations in the application of UAV in large areas due to small battery capacity and safety reasons. Therefore, the UAV based system can only measure the atmospheric quality at discrete points and at certain time instances within the small space of deep open-cast mines. To overcome this limitation, identification of the suitable interpolation method based on observation data from UAV monitoring system is necessary.

Spatial interpolation is a method that best represents the whole space and predicts the values at points where observation data is unavailable (Lam, 1983). This method assumes the data is continuous over the area and spatially dependent, indicating that values closer together are more likely to be similar than the values further apart. The goal of spatial interpolation is to create a surface representing as close as the true one. There are several interpolation methods such as trilinear interpolation, natural neighbour, and nearest neighbour, which



Fig. 1. Location of study area and its landscape  
Rys. 1. Położenie badanego obszaru i jego krajobraz



Fig. 2. DJI Inspire 2 UAV  
Rys. 2. BSP DJI Inspire 2

were commonly used to visualize and mapping substances in the three-dimension (3D) space. However, different methods may provide different interpolated results depending on the characteristics of observed data, especially the number of sampling points. Thus, in order to provide an accurate estimation of air quality based on air sampling points collected by the UAV based method, a testing and validating interpolation method is needed (Espitia-Pérez et al., 2018).

To have a deep insight into air quality in mining sites, this study is to seek an approach that could accurately estimate the 3D concentration of several air compositions in open-pit coal mines based upon the UAV monitoring system. To achieve this objective, different interpolation methods were tested with observation data acquired by the UAV monitoring system. The most suitable method for constructing 3D distribution of air quality was chosen based upon cross-validation with four errors including mean error (ME), mean absolute error (MAE), root mean square error (RMSE), and percent error (PE).

## 2. Study area and data collection

### 2.1 Study area

Deo Nai open-pit coal mine was selected for this study. It is located in the northern part of Vietnam (Fig 1). The mine is managed by the Deo Nai Joint Stock Coal Company which was established on 1st August 1960 by the Decision 707 BCN/VB on 27th July 1960. Coal extracted from this mine has the highest quality in the north-eastern coal basin. According to the permission decision of exploitation (2817/GP-BTNMT) issued by the Ministry of Natural Resources and Environment in 2008, the mine has a maximum area of 6.06 km<sup>2</sup> and a reservation of 42 500 000 ton producing 2 500 000 ton per year. The Deo Nai open-pit coal mine intends to close in the year of 2025 when it reaches to the minimum extraction elevation of -345 m above from the sea level (amsl). At present, the mine has reached to the minimum extraction elevation of -150 m amsl with bench height, bench width, and working slope varying from 20 to 30 m, 40 to 70 m, and from 24o to 32o, respectively (Bien, 2015). In this study site, the main mining

activities include drilling, blasting, loading, and hauling operations emitting different particle matters, especially PM<sub>2.5</sub> and hazardous gases (CO, CO<sub>2</sub>, and SO<sub>2</sub>) which may directly impact on workers' health. Therefore, the accurate estimation of air quality distribution in three directions is necessary.

### 2.2 Data collection

#### a. UAV platform

In this study, a DJI Inspire 2 drone (Fig 2) was used for air quality monitoring. The drone's technical parameters are presented in Table 1 (<https://www.dji.com/inspire-2/info>). It can be seen from Table 1 that DJI Inspire 2 can take off with an 810 g object. This allows the drone flying safely with air sensors mounted on it. However, its flight time decreases.

Electrochemistry sensors and laser dust sensor were used to evaluate four major pollutants, including PM<sub>2.5</sub>, CO, CO<sub>2</sub>, and SO<sub>2</sub> (Fig 3a). Technical parameters of those sensors are described in Table 2. The sensors were attached to the drone for monitoring several components of air and called UAV multi-sensor collectors (UAV-MSC) system. Due to the load limitation of UAV, light and compact sensors were packed in a perforated box and mounted on the vehicle (Fig 3b). Data were stored in a SD card.

#### b. Air quality sensors

Electrochemistry sensors and laser dust sensor were used to evaluate four major pollutants, including PM<sub>2.5</sub>, CO, CO<sub>2</sub>, and SO<sub>2</sub> (Fig 3a). Technical parameters of those sensors are described in Table 2. The sensors were attached to the drone for monitoring several components of air and called UAV multi-sensor collectors (UAV-MSC) system. Due to the load limitation of UAV, light and compact sensors were packed in a perforated box and mounted on the vehicle (Fig 3b). Data were stored in a SD card.

#### c. Description of data collection

Due to the limited battery capacity, the UAV has less hovering time with more load. A total load of sensors and oth-

Tab. 1. Specifications of drone  
 Tab. 1. Techniczne specyfikacje drona

Name of UAV	DJI Inspire 2
Weight	3440 g
Battery	6000 mAh
Max flight time	Approx. 27 min
Cruise speed	- P mode/A-mode: 16.4 ft/s (5 m/s) - S-mode: 19.7 ft/s (6 m/s)
Radio link range	7 km
Payload	4250 g

Tab. 2. Specifications of the air quality monitoring sensors  
 Tab. 2. Specyfikacje czujników monitorujących jakość powietrza

Parameters	Sensor category	Range	Precision	Resolution
PM <sub>2.5</sub>	Laser dust sensor	0-500 µg/m <sup>3</sup>	± 10%	0.3 µg/m <sup>3</sup>
CO	Electrochemistry sensor	0-750ppm	± 5% ppm	1 ppm
CO <sub>2</sub>	Electrochemistry sensor	0-750ppm	± 5% ppm	1 ppm
SO <sub>2</sub>	Electrochemistry sensor	0-20ppm	± 5% ppm	0.1 ppm

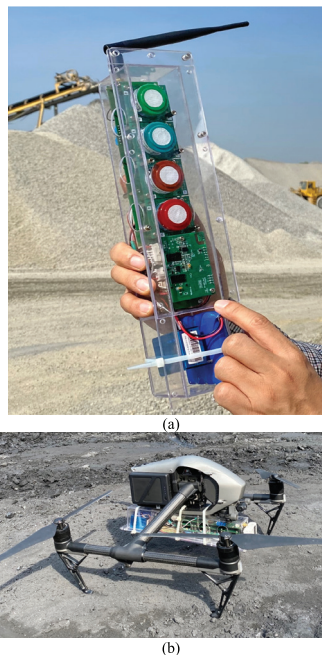


Fig. 3. (a) Sensors and (b) modular gas-sensor system mounted  
 Rys. 3. (a) Zamontowane czujniki i (b) modułowy system czujników gazu

er accessories was 0.8 kg corresponding to the flight time of 25 minutes, including taking off and landing. Therefore, the working time of the UAV monitoring system is approximately 15 minutes. Figure 4 and Figure 5a depict the preparation of taking off and the UAV flight paths to measure air components within the pit. UAV flew in the space of the study mine with an average speed of 4 m/s. At the same time, the velocity and direction of wind were also measured. The data collected were utilized to make 3D air models.

### 3. Methods

#### Spatial interpolation methods

In order to accurately predict the spatial distribution of air quality in the study site, three spatial interpolation methods including trilinear interpolation, nearest neighbour, and natural neighbour were tested and evaluated using UAV observation data and based on different performance indexes.

#### a) Trilinear interpolation

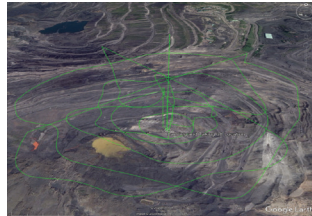
Trilinear is an extension of the linear interpolation performed with points within a box (3D) given values at the vertices of the box (Bourke, 1999). With two adjacent data points, each line is formed and can be interpolated independently. Suppose  $(x_i; y_i)$  and  $(x_{i+1}; y_{i+1})$  are the previous and latter endpoints of a line segment, respectively. For the point where the abscissa is  $x$ , and its  $y$  is:

$$y = y_i + (y_{i+1} - y_i) \frac{x - x_i}{x_{i+1} - x_i} \quad (1)$$

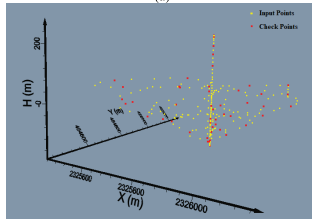
When input parameters are multidimensional, bilinear interpolation or trilinear interpolation is required. Bilinear interpolation is a linear interpolation with two variables. The main idea is to perform interpolation calculation (Eq. 1) respectively in directions of the two variables. The trilinear interpolation is able to add one direction (or variable) based on the bilinear interpolation (Fig 6) (Cam Q. T. Thanh, 2017).



Fig. 1. Location of study area and its landscape  
Rys. 1. Położenie badanego obszaru i jego krajobraz



(a)



(b)

Fig 5. (a) Flight paths; (b) Air monitoring points  
Rys. 5. (a) Trasy lotu; b) Punkty monitorowania powietrza

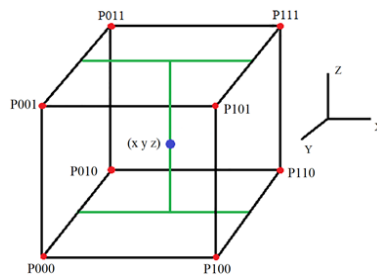
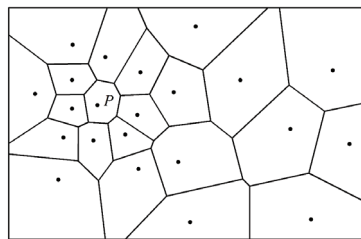
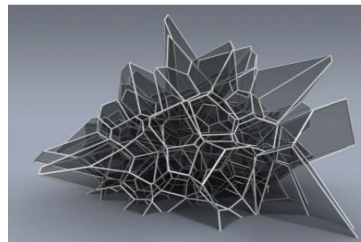


Fig. 6. Representation of a trilinear interpolation model (modified from Cam Q. T. Thanh (2017))  
Rys. 6. Reprezentacja trójliniowego modelu interpolacyjnego



(a)



(b)

Fig. 7. (a) 2D Voronoi diagram; (b) 3D Voronoi diagram (Liu, Zhu, Wang, & Liu, 2010)  
Rys. 7. (a) Diagram Woronoja 2D; (b) Diagram 3D Woronoija (Liu, Zhu, Wang i Liu, 2010)

Tab. 3. Cross-validation test result for PM2.5 estimates  
 Tab. 3. Wyniki testu walidacji krzyżowej dla oszacowań PM2.5

Method of interpolation	Mean error (ME)	Mean absolute error (MAE)	Root mean square error (RMSE)	PE (%)
Trilinear	-0.116	4.787	5.896	15.2
Nearest Neighbor	0.250	5.750	7.141	18.4
Natural Neighbor	-0.516	5.014	6.274	16.2

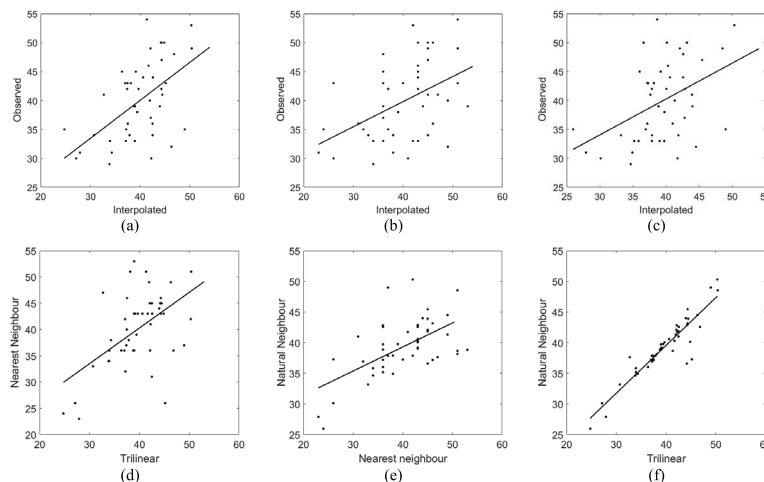


Fig 8. Scatter diagrams of observed and estimated concentrations for PM2.5 with (a) Trilinear interpolation; (b) Nearest Neighbor; (c) Natural Neighbor. Scatter diagrams of estimated concentrations for PM2.5 by (d) Nearest Neighbor and Trilinear; (e) Natural neighbour and Nearest neighbour; (f) Natural Neighbour and Trilinear

Rys. 8. Diagramy rozrzutu obserwowanych i szacunkowych stężeń PM2.5 z (a) Interpolacją Trójliniową; (b) Najbliższym sąsiadem; (c) Naturalnym Sąsiadem. Diagramy rozrzutu szacowanych stężeń pyłu PM2.5 według: (d) Najbliższego Sąsiada i Trójliniowego; (e) Naturalnego Sąsiada i Najbliższego Sąsiada; (f) Naturalnego Sąsiada i Trójliniowego

Tab. 4. Cross-validation test result for CO estimates  
 Tab. 4. Wyniki testu walidacji krzyżowej dla oszacowań CO

Method of interpolation	Mean error (ME)	Mean absolute error (MAE)	Root mean square error (RMSE)	PE (%)
Trilinear	0.058	0.102	0.192	10.3
Nearest Neighbor	0.040	0.145	0.295	15.8
Natural Neighbor	0.066	0.118	0.210	11.3

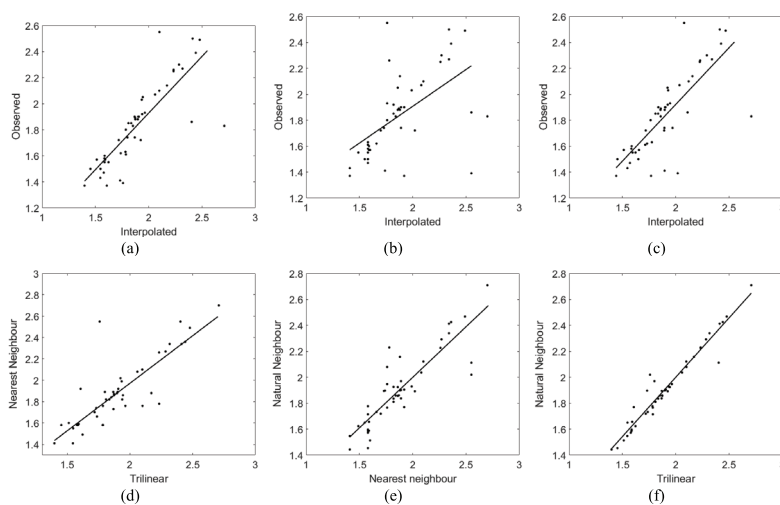


Fig 8. Scatter diagrams of observed and estimated concentrations for PM2.5 with (a) Trilinear interpolation; (b) Nearest Neighbor; (c) Natural Neighbor. Scatter diagrams of estimated concentrations for PM2.5 by (d) Nearest Neighbor and Trilinear; (e) Natural neighbour and Nearest neighbour; (f) Natural Neighbour and Trilinear

Rys. 8. Diagramy rozrzutu obserwowanych i szacunkowych stężeń PM2.5 z (a) Interpolacją Trójliniową; (b) Najbliższym sąsiadem; (c) Naturalnym Sąsiadem. Diagramy rozrzutu szacowanych stężeń pyłu PM2.5 według: (d) Najbliższego Sąsiada i Trójliniowego; (e) Naturalnego Sąsiada i Najbliższego Sąsiada; (f) Naturalnego Sąsiada i Trójliniowego



Tab. 5. Cross-validation test result for SO<sub>2</sub> estimates  
 Tab. 5. Wyniki testu walidacji krzyżowej dla oszacowań SO<sub>2</sub>

Method of interpolation	Mean error (ME)	Mean absolute error (MAE)	Root mean square error (RMSE)	PE (%)
Trilinear	0.007	0.011	0.019	12.9
Nearest Neighbor	0.005	0.019	0.031	20.6
Natural Neighbor	0.008	0.012	0.021	14.3

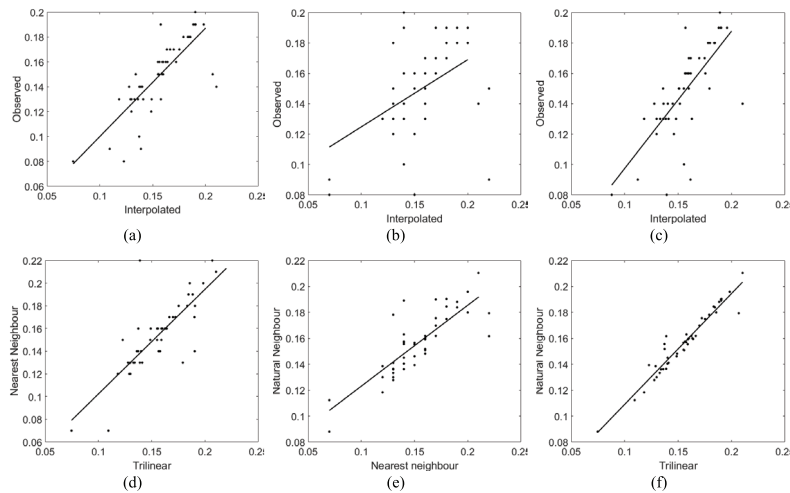


Fig 10. Scatter diagrams of observed and estimated concentrations for SO<sub>2</sub> with (a) Trilinear interpolation; (b) Nearest Neighbour; (c) Natural Neighbor; Scatter diagrams of estimated concentrations for SO<sub>2</sub> by: (d) Nearest Neighbor and Trilinear; (e) Natural neighbour and Nearest neighbour; (f) Natural Neighbor and Trilinear

Rys. 10. Diagramy rozrzutu obserwowanych i szacowanych stężeń SO<sub>2</sub> z (a) Interpolacją Trójliniową; (b) Najbliższym sąsiadem; (c) Naturalny Sąsiadem; Diagramy rozrzutu szacowanych stężeń SO<sub>2</sub> według: (d) Najbliższego Sąsiada i Trójliniowego; (e) Naturalnego Sąsiada i Najbliższego Sąsiada; (f) Naturalnego Sąsiada i Trójliniowego

Tab. 6. Cross-validation test result for CO<sub>2</sub> estimates  
 Tab. 6. Wyniki testu walidacji krzyżowej dla oszacowań CO<sub>2</sub>

Method of interpolation	Mean error (ME)	Mean absolute error (MAE)	Root mean square error (RMSE)	PE (%)
Trilinear	4.428	14.086	19.189	3.7
Nearest Neighbor	7.208	18.458	26.894	5.2
Natural Neighbor	5.631	15.396	19.702	3.8

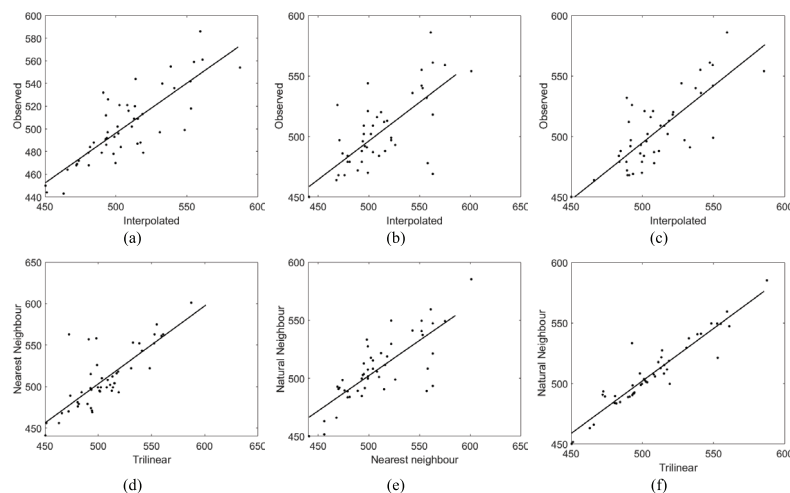


Fig. 11. Nearest Neighbor; (c) Natural Neighbor; Scatter diagrams of estimated concentrations for CO<sub>2</sub> by (d) Nearest Neighbor and Trilinear; (e) Natural neighbour and Nearest neighbour; (f) Natural Neighbor and Trilinear

Rys. 11. Diagramy rozrzutu obserwowanych i szacowanych stężeń CO<sub>2</sub> z (a) Interpolacją Trójliniową; (b) Najbliższym Sąsiadem; (c) Naturalnym Sąsiadem; Diagramy rozrzutu szacowanych stężeń CO<sub>2</sub> według: (d) Najbliższego Sąsiada i Trójliniowego; (e) Naturalnego Sąsiada i Najbliższego Sąsiada; (f) Naturalnego Sąsiada i Trójliniowego

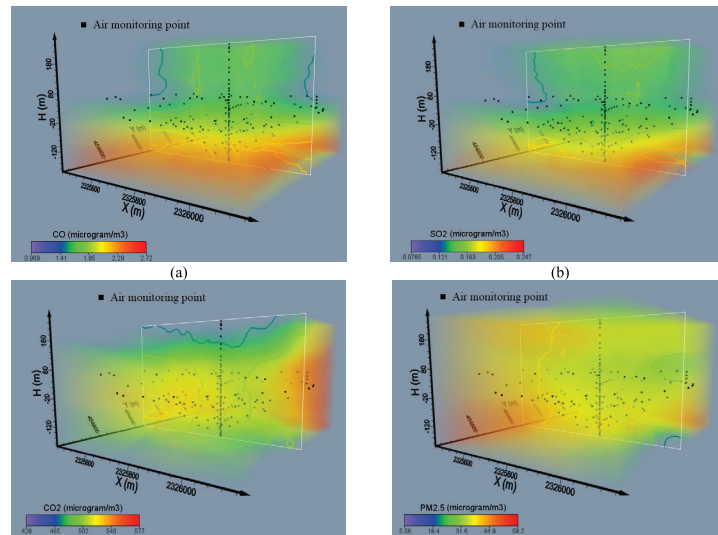


Fig. 12. Volume rendering and contour plots created using the trilinear interpolation method  
 Rys. 12. Renderowanie objętości i wykresy konturowe utworzone metodą interpolacji trójliniowej

$$P_{xyz} = P_{000}(1-x)(1-y)(1-z) + P_{100}x(1-y)(1-z) + P_{010}(1-x)y(1-z) + P_{001}(1-x)(1-y)z + P_{101}(1-x)yz + P_{110}(1-y)xz + P_{110}xy(1-z) \quad (2)$$

where  $P_{xyz}$  is the value of sampled point at coordinates (xyz).

#### b) Nearest neighbour

Nearest interpolation is the simplest interpolation method. The main idea of this method is that the interpolated point receives the value of its closest sampled point. Therefore, in the processing, it is to find a point closest to the interpolation point before assigning the value of the point to the interpolation point.

The performance of this interpolation requires the space surrounding a sampled point to be decomposed into cells called a Voronoi diagram, so at any points in this space, the closest given point is inside this cell. The graphic representation of a Voronoi diagram in both 2D and 3D is shown in the Fig 7a and 7b, respectively.

#### c. Natural neighbour

This is a local interpolant which is also based on the Voronoi diagram, as shown in Figure 7. Its estimation function is a linear and appropriately weighted average of the nearby data points or natural neighbours. The method of selecting natural neighbours and the interpolation weights was proposed by Sibson (1981). According to this method, initially, for a given set of irregular points  $P = (P_1 \dots P_n)$ , the original Voronoi diagram is constructed; subsequently, the target interpolation point  $q$  is inserted in the diagram, altering the Voronoi diagram. The point  $q$  in the new Voronoi diagram is associated with the region  $V(q)$  and the interpolation weights  $w_i$  were calculated as Eq.3 (Quanfu Fan, 2005) below:

$$w_i = \frac{Area(V(q) \cap V(P_i))}{Area(V(q))} \quad (3)$$

where  $P_i$  the natural neighbours of  $q$  and  $V(P_i)$  their associated regions in the original Voronoi diagram. The natural and the nearest neighbour schemes belong to the polygonal interpolation group of methodologies and are local, deterministic,

and abrupt schemes.

#### Accuracy assessment

The cross-validation was used; this is a common validation in environmental research (Goutham Priya M, 2018; Jha et al., 2011; Kurtzman & Kadmon, 1999). For each interpolation method, we employed 80% of the observed data to calculate the concentration of air components for a number of 20 % points after excluding them from the input data.

The interpolation of air quality distribution was evaluated using mean error (ME), mean absolute error (MAE) and root mean square error (RMSE). ME indicates the predictive lack of bias, while MAE provides a measure of how far the estimate can be in error, ignoring sign (Hulme et al., 1995). The RMSE provides a measure that is sensitive to outliers (Nalder & Wein, 1998). The ME, MAE, RMSE were estimated based on the Eq.4, Eq.5, and Eq.6, respectively.

$$MAE = \frac{1}{N} \sum_{i=1}^N |P_i - P_i^*| \quad (4)$$

$$ME = \frac{1}{N} \sum_{i=1}^N (P_i - P_i^*) \quad (5)$$

$$RMSE = \sqrt{\frac{1}{N} \sum_{i=1}^N (P_i - P_i^*)^2} \quad (6)$$

In addition, the cross-validation method is based on percent error or PE (%), which is defined as Eq.7:

$$PE(\%) = \frac{RMSE}{\left(\frac{1}{N}\right) \sum_{i=1}^N P_i^*} \times 100(\%) \quad (7)$$

Where RMSE is the mean of the squared difference between the observed value ( $P_i^*$ ) and the predicted value ( $P_i$ ), and  $N$  is the number of observations. The smaller the value, the more accurate the method is.

## 4. Results and discussions

### 4.1. Comparative analysis of interpolation methods

During the monitoring period, there was no mining operation because it was the break time between morning and afternoon shifts. Also, there was almost no wind within the

space of the study open-pit mine as it is extremely deep and steep. The wind velocity was recorded around 0.4 m/s, the humidity varied from 73 to 81%, and temperature recorded around 27°C. The monitoring points are depicted in Fig 5b.

Figures 8-12 depict scatter plots which are presented for each of three methods. In Figures 8d-f, 9d-f, 10d-f, 11d-f, and 12d-f we can see that trilinear interpolation (TI) and natural neighbour (NaNe) performed similarly, whereas there are clearly differences in the performance between TI and nearest neighbour (NeN) and between NaNe and NeN.

For numerical analysis, as stated in Tables 3-6 for all four air compositions, TI shows the lowest errors followed by NaNe while NeN produced the results with the largest errors. In addition, the performance of three interpolation methods for CO<sub>2</sub> is the best based on PE. Specifically, trilinear interpolation of CO<sub>2</sub> gave a PE of 3.7% which was smaller than that of CO, SO<sub>2</sub>, and PM2.5 with 10.3%, 12.9%, and 15.2%, respectively.

For the interpolation of PM2.5, Table 3 shows that TI performed the best with the lowest errors of -0.116 (ME), 4.787 (MAE) and 5.896 (RMSE), whereas NeN produced the worst results with the largest errors of -0.516 (ME), 5.014 (MAE), and 7.141 (RMSE).

For estimation of CO concentration, Table 4 shows that TI produced the lowest errors of 0.058 (ME), 0.102 (MAE) and 0.295 (RMSE), whereas NeN produced the largest errors of 0.040 (ME), 0.145 (MAE), and 0.295 (RMSE). Similarly, for SO<sub>2</sub>, the ME, MAE, and RMSE varied from 0.005 to 0.008, 0.011 to 0.019, and 0.019 to 0.031, respectively (Table 5). Finally, the ME, MAE, and RMSE for CO<sub>2</sub> varied from 4.428 to 7.208, 14.086 to 18.458, and 19.189 to 26.702, respectively (Table 6).

#### 4.2. Estimation of 3D air quality distribution

As illustrated in the previous section, the TI method performed the highest accurate estimation result compared the others, therefore it was used to reconstruct a 3D distribution of different emissions in the study site based on the measured data from UAV multi-sensor collectors (UAV-MS). The location of each sampling point was identified using VN-2000 coordinate. In each model, a ZY profile was also created to show contours of interpolated values. Figure 11 showed a 3D distribution of four air pollutant substances using software Voxel. The concentration of four toxic emissions (CO, SO<sub>2</sub>, CO<sub>2</sub>, and PM2.5) showed a relatively wide variation ranging from 0.969÷2.72 µg/m<sup>3</sup> (CO), 0.0785÷0.247 µg/m<sup>3</sup> (SO<sub>2</sub>), 428÷577 µg/m<sup>3</sup> (CO<sub>2</sub>), and 5.06÷58.2 µg/m<sup>3</sup> (PM2.5). More noticeably, although two most of the toxic chemicals (CO and SO<sub>2</sub>)

have a lower concentration of 0.247 µg/m<sup>3</sup> and 2.47 µg/m<sup>3</sup>, the high concentration at the bottom of the pit may harmfully impact on occupational health, especially who works for a long-time in deeper areas of open-pit mines. Meanwhile, CO<sub>2</sub> and PM2.5 distributed entirely in the open-pit area, which not only impacts on the working environment but increases environmental risks in surrounding areas. These findings provide additional evidence explaining regional pollution caused by mining activities in many countries worldwide (Gautam et al., 2018; Hendryx et al., 2020). It also raises the necessity of reducing air pollution in mining sites to prevent health-related issues in both local and regional scales.

#### Conclusion

This study presents a new approach to flexibly monitor and accurately estimate air quality in an open-pit coal mine. It was built based on constructing the UAV multi-sensor collectors (UAV-MS) system and testing different interpolation methods for establishing a 3D distribution of four toxic emissions from the open-pit coal mine. UAV-MS system shows the practical ability to carry various sensors to monitor air quality in open-pit coal mines. It can be used to measure different air quality components (PM2.5, CO, CO<sub>2</sub>, and SO<sub>2</sub>). Moreover, the system works safely and effectively in the condition of open-pit mines compared to conventional ground-based monitoring systems which often cost a high price and are difficult to monitor air quality following vertical direction.

Also, different interpolation methods, namely trilinear interpolation, nearest neighbour, and the natural neighbour were applied to reproduce the vertical distribution of toxic emissions based on measured data from the UAV-MS system. To evaluate these interpolation methods, the cross-validation method with four errors including mean error, mean absolute error, root mean square error and percent error were used. The results show that trilinear interpolation is the most suitable method for spatial modelling of air components in the three dimensions of space as this method gave the smallest errors compared to the two remaining methods.

In short, the proposed approach provides an additional option with simple procedures and acceptable price to measure flexibility an estimate accurately 3D distribution of air quality in open-pit mines.

#### Acknowledgements

This research was supported by the Ministry of Education and Training of Vietnam (MOET) under grant number B2018-MDA-03SP.



## Literatura – References

1. Alvarado, M., Gonzalez, F., Fletcher, A., & Doshi, A. (2015). Towards the Development of a Low Cost Airborne Sensing System to Monitor Dust Particles after Blasting at Open-Pit Mine Sites. *Sensors (Basel, Switzerland)*, 15(8), 19667-19687. doi:10.3390/s150819667.
2. Arregocés, H. A., Rojano, R., Angulo, L., & Restrepo, G. (2018). Intake Fraction of PM<sub>10</sub> from Coal Mine Emissions in the North of Colombia. *Journal of Environmental and Public Health*, 2018, 8532463. doi:10.1155/2018/8532463.
3. Bien, N. V. (2015). Research and recommendations on solutions for the improvement of productivity and reducing the prices of coal in Vinacomin (in Vietnamese).
4. Bourke, P. (1999). Interpolation methods. *Miscellaneous: projection, modelling, rendering*, 1, 10.
5. Bui, D. T., Long, N. Q., Bui, X.-N., Nguyen, V.-N., Van Pham, C., Van Le, C., . . . Kristoffersen, B. (2017). Light-weight Unmanned Aerial Vehicle and Structure-from-Motion Photogrammetry for Generating Digital Surface Model for Open-Pit Coal Mine Area and Its Accuracy Assessment. Paper presented at the International Conference on Geo-Spatial Technologies and Earth Resources.
6. Bui, X.-N., Choi, Y., Atrushkevich, V., Nguyen, H., Tran, Q.-H., Long, N. Q., & Hoang, H.-T. (2020). Prediction of Blast-Induced Ground Vibration Intensity in Open-Pit Mines Using Unmanned Aerial Vehicle and a Novel Intelligence System. *Natural Resources Research*, 29(2), 771-790. doi:10.1007/s11053-019-09573-7
7. Cam Q. T. Thanh, N. T. H. (2017). Trilinear Interpolation Algorithm for Reconstruction of 3D MRI Brain Image. *American Journal of Signal Processing*, 7(1), 11.
8. Chang, C.-C., Chang, C.-Y., Wang, J.-L., Pan, X.-X., Chen, Y.-C., & Ho, Y.-J. (2020). An optimized multicopter UAV sounding technique (MUST) for probing comprehensive atmospheric variables. *Chemosphere*, 254, 126867. doi:https://doi.org/10.1016/j.chemosphere.2020.126867.
9. Chen, D., Feng, Q., Liang, H., Gao, B., & Alam, E. (2019). Distribution characteristics and ecological risk assessment of polycyclic aromatic hydrocarbons (PAHs) in underground coal mining environment of Xuzhou. *Human and Ecological Risk Assessment: An International Journal*, 25(6), 1564-1578. doi:10.1080/10807039.2018.1489715.
10. Dieu Hien, V. T., Lin, C., Thanh, V. C., Kim Oanh, N. T., Thanh, B. X., Weng, C.-E., . . . Rene, E. R. (2019). An overview of the development of vertical sampling technologies for ambient volatile organic compounds (VOCs). *Journal of Environmental Management*, 247, 401-412. doi:https://doi.org/10.1016/j.jenvman.2019.06.090.
11. Espitia-Pérez, L., Arteaga - Pertuz, M., Soto, J. S., Espitia-Pérez, P., Salcedo-Arteaga, S., Pastor-Sierra, K., . . . Henriques, J. A. P. (2018). Geospatial analysis of residential proximity to open-pit coal mining areas in relation to micronuclei frequency, particulate matter concentration, and elemental enrichment factors. *Chemosphere*, 206, 203-216. doi:https://doi.org/10.1016/j.chemosphere.2018.04.049.
12. Gautam, S., Patra, A. K., Sahu, S. P., & Hitch, M. (2018). Particulate matter pollution in opencast coal mining areas: a threat to human health and environment. *International Journal of Mining, Reclamation and Environment*, 32(2), 75-92. doi:10.1080/17480930.2016.1218110.
13. Goutham Priya M, J. S. (2018). Evaluation of Interpolation Techniques for Air Quality Monitoring using Statistical Error Metrics: A Review. *INTERNATIONAL JOURNAL OF ENGINEERING RESEARCH & TECHNOLOGY (IJERT)*, 6(7).
14. Grozdanovic, M., Bijelić, B., & Marjanovic, D. (2018). Impact assessment of risk parameters of underground coal mining on the environment. *Human and Ecological Risk Assessment: An International Journal*, 24(4), 1003-1015. doi:10.1080/10807039.2017.1405339.
15. Hendryx, M., Islam, M. S., Dong, G.-H., & Paul, G. (2020). Air Pollution Emissions 2008–2018 from Australian Coal Mining: Implications for Public and Occupational Health. *International Journal of Environmental Research and Public Health*, 17(5). doi:10.3390/ijerph17051570.
16. Hulme, M., Conway, D., Jones, P. D., Jiang, T., Barrow, E. M., & Turney, C. (1995). Construction of a 1961–1990 European climatology for climate change modelling and impact applications. *International Journal of Climatology*, 15(12), 1333-1363. doi:10.1002/joc.3370151204.
17. Jha, D., M.Sabesan, Das, A., Vinithkumar, N. V., & Kirubakaran, R. (2011). Evaluation of Interpolation Technique for Air Quality Parameters in Port Blair, India. *Universal Journal of Environmental Research and Technology* 2249-0256, 1, 301-310.
18. Kurtzman, D., & Kadmon, R. (1999). Mapping of temperature variables in Israel: a comparison of different interpolation methods. *Climate Research*, 13, 33-43. doi:10.3354/cr013033.
19. Lam, N. S.-N. (1983). Spatial Interpolation Methods: A Review. *The American Cartographer*, 10(2), 22.

20. Le, C. V., Cao, C.Xuan, Le, V.Hong & Dinh, T. (2020). Volume computation of quarries in Vietnam based on Unmanned Aerial Vehicle (UAV) data. *Journal of Mining and Earth Sciences*, 61(1), 10. doi:[https://doi.org/10.46326/JMES.2020.61\(1\).03](https://doi.org/10.46326/JMES.2020.61(1).03).
21. León-Mejía, G., Espitia-Pérez, L., Hoyos-Giraldo, L. S., Da Silva, J., Hartmann, A., Henriques, J. A. P., & Quintana, M. (2011). Assessment of DNA damage in coal open-cast mining workers using the cytokinesis-blocked micronucleus test and the comet assay. *Science of the Total Environment*, 409(4), 686-691. doi:10.1016/j.scitotenv.2010.10.049.
22. Liu, C., Huang, J., Wang, Y., Tao, X., Hu, C., Deng, L., . . . Xiao, W. (2020). Vertical distribution of PM2.5 and interactions with the atmospheric boundary layer during the development stage of a heavy haze pollution event. *Science of the Total Environment*, 704, 135329. doi:<https://doi.org/10.1016/j.scitotenv.2019.135329>.
23. Long, J., Tan, D., Deng, S., & Lei, M. (2018). Pollution and ecological risk assessment of antimony and other heavy metals in soils from the world's largest antimony mine area, China. *Human and Ecological Risk Assessment: An International Journal*, 24(3), 679-690. doi:10.1080/10807039.2017.1396531.
24. Long, N. Q., Nam, B. X., Cuong, C. X., & Canh, L. V. (2019). An approach of mapping quarries in Vietnam using low-cost Unmanned Aerial Vehicles. 11(2), 199-210. doi: 10.21177/1998-4502-2019-11-2-199-210.
25. Nalder, I. A., & Wein, R. W. (1998). Spatial interpolation of climatic Normals: test of a new method in the Canadian boreal forest. *Agricultural and Forest Meteorology*, 92(4), 211-225. doi:10.1016/S0168-1923(98)00102-6.
26. Nghia, N. V. (2020). "Building DEM for deep open-pit coal mines using DJI Inspire 2. *Journal of Mining and Earth Sciences*, 61(1), 1-10. doi:10.46326/JMES.2020.61(1).01.
27. Padró, J.-C., Carabassa, V., Balagué, J., Brotons, L., Alcañiz, J. M., & Pons, X. (2019). Monitoring opencast mine restorations using Unmanned Aerial System (UAS) imagery. *Science of the Total Environment*, 657, 1602-1614. doi:<https://doi.org/10.1016/j.scitotenv.2018.12.156>.
28. Pandey, B., Agrawal, M., & Singh, S. (2014). Assessment of air pollution around coal mining area: Emphasizing on spatial distributions, seasonal variations and heavy metals, using cluster and principal component analysis. *Atmospheric Pollution Research*, 5(1), 79-86. doi:<https://doi.org/10.5094/APR.2014.010>.
29. Petsonk, E. L., Rose, C., & Cohen, R. (2013). Coal mine dust lung disease. New lessons from old exposure. *American journal of respiratory and critical care medicine*, 187(11), 1178-1185. doi:10.1164/rccm.201301-0042CI.
30. Quanfu Fan, A. E., Vladlen Koltun, Shankar Krishnan, Suresh Venkatasubramanian. (2005, Jan 22 2005 → Jan 22 2005). Hardware-assisted natural neighbor interpolation. Paper presented at the the Seventh Workshop on Algorithm Engineering and Experiments and the Second Workshop on Analytic Algorithms and Combinatorics, Vancouver, BC, Canada.
31. Raeva, P. L., Filipova, S. L., & Filipov, D. G. (2016). Volume Computation of a Stockpile - a Study Case Comparing GPS and Uav Measurements in AN Open Pit Quarry. *ISPRS - International Archives of the Photogrammetry, Remote Sensing and Spatial Information Sciences*, 41B1, 999. Retrieved from <https://ui.adsabs.harvard.edu/abs/2016ISPA41B1..999R>.
32. Rohi, G., Ejofodomi, O. t., & Ofualagba, G. (2020). Autonomous monitoring, analysis, and countering of air pollution using environmental drones. *Heliyon*, 6(1), e03252. doi:<https://doi.org/10.1016/j.heliyon.2020.e03252>
33. Sheng, Q., Zhang, Y., Zhu, Z., Li, W., Xu, J., & Tang, R. (2019). An experimental study to quantify road greenbelts and their association with PM2.5 concentration along city main roads in Nanjing, China. *Science of the Total Environment*, 667, 710-717. doi:<https://doi.org/10.1016/j.scitotenv.2019.02.306>.
34. Sibson, R. (1981). A brief description of natural neighbor interpolation. *Computer Science*, 15.
35. Villa, T. F., Salimi, F., Morton, K., Morawska, L., & Gonzalez, F. (2016). Development and Validation of a UAV Based System for Air Pollution Measurements. *Sensors*, 16(12). doi:10.3390/s16122202.
36. Yang, J.-H., Jung, J., Ryu, J.-H., & Yoh, J. J. (2020). Real-time monitoring of toxic components from fine dust air pollutant samples by utilizing spark-induced plasma spectroscopy. *Chemosphere*, 257, 127237. doi:<https://doi.org/10.1016/j.chemosphere.2020.127237>.
37. Zhang, X., Bai, X., Li, C., Li, T., Wang, R., Zhao, Z., & Norback, D. (2020). Elemental composition of ambient air particles in Taiyuan, China: evaluation of lifetime cancer and non-cancer risks. *Human and Ecological Risk Assessment: An International Journal*, 26(5), 1391-1406. doi:10.1080/10807039.2019.1579048.

### *Metody interpolacji przestrzennej 3D dla oceny jakości powietrza w kopalniach odkrywkowych z danymi uzyskanymi przez system monitorowania oparty na pospolitym bezzałogowym statku powietrznym BSP*

*Wielorakie działalności u górnictwie odkrywkowym, w tym roboty strzelnicze, wiertnicze, załadowania, transport, zwałowania itp. często prowadzi do bezpośredniej emisji pyłów i gazów do atmosfery. Zanieczyszczenie powietrza na terenie zakładu górniczego uważane jest za zagrożenie dla zdrowia pracowników i górników, zwłaszcza ryzyko rozwoju chorób układu oddechowego. Aby zidentyfikować te potencjalne zagrożenia, niezbędny jest system monitorowania jakości powietrza i analiza przestrzenna. W artykule, przedstawiono wyniki zastosowania system monitorowania jakości powietrza, który integruje czujniki gazu i pyłu w pospolitym wielowirnikowym helikopterze lub bezzałogowym statku powietrznym (BSP). Zbadano również różne metody interpolacji przestrzennej, w tym interpolację trójliniową, najbliższego sąsiada i naturalnego sąsiada, zastosowane do danych z monitoringu (CO, SO<sub>2</sub>, PM<sub>2.5</sub>, CO<sub>2</sub>) z badanego systemu w celu wyznaczenia poziomów stężenia powietrza w atmosferze kopalni odkrywkowych. Wyniki pokazują, że system monitorowania jakości powietrza oparty na BSP działał sprawnie i bezpiecznie w warunkach głębokich odkrywkowych kopalń węgla kamiennego. Dodatkowo, do oszacowania poziomu stężeń gazów i pyłów w niepróbkowanych punktach zastosowano interpolację trójliniową z najdokładniejszym wynikiem, a po kolei naturalny sąsiad i najbliższy sąsiad.*

**Słowa kluczowe:** *jakość powietrza, kopalnie odkrywkowe, interpolacja przestrzenna, bezzałogowe statki powietrzne (BSP)*